Acta Biomaterialia xxx (xxxx) xxx

Contents lists available at ScienceDirect

Acta Biomaterialia

journal homepage: www.elsevier.com/locate/actbio

Full length article

Electrically responsive release of proteins from conducting polymer hydrogels

Ernest Cheah[a], Mahima Bansal[a], Linh Nguyen[b], Anaïs Chalard[c], Jenny Malmström[d,e], Simon J. O'Carroll[e], Bronwen Connor[b], Zimei Wu[a], Darren Svirskis[a,*]

[a] School of Pharmacy, Faculty of Medical and Health Sciences, University of Auckland, Private Bag 92019, Auckland, New Zealand
[b] Department of Pharmacology and Clinical Pharmacology, School of Medical Sciences Faculty of Medical and Health Sciences, University of Auckland, Private Bag 92019, Auckland, New Zealand
[c] Department of Chemical and Materials Engineering, University of Auckland, Private Bag 92019, Auckland 1142, New Zealand
[d] MacDiarmid Institute for Advanced Materials and Nanotechnology, Victoria University of Wellington, P.O. Box 600, Wellington 6140, New Zealand
[e] Department of Anatomy and Medical Imaging, School of Medical Sciences, Faculty of Medical and Health Sciences, University of Auckland, Private Bag 92019, Auckland, New Zealand

ARTICLE INFO

Article history:
Received 29 August 2022
Revised 21 December 2022
Accepted 5 January 2023
Available online xxx

Keywords:
PEDOT
GelMA
Electric stimuli
Growth factors
Electroactive materials

ABSTRACT

Electrically modulated delivery of proteins provides an avenue to target local tissues specifically and tune the dose to the application. This approach prolongs and enhances activity at the target site whilst reducing off-target effects associated with systemic drug delivery. The work presented here explores an electrically active composite material comprising of a biocompatible hydrogel, gelatin methacryloyl (GelMA) and a conducting polymer, poly(3,4-ethylenedioxythiophene), generating a conducting polymer hydrogel. In this paper, the key characteristics of electroactivity, mechanical properties, and morphology are characterized using electrochemistry techniques, atomic force, and scanning electron microscopy. Cytocompatibility is established through exposure of human cells to the materials. By applying different electrical-stimuli, the short-term release profiles of a model protein can be controlled over 4 h, demonstrating tunable delivery patterns. This is followed by extended-release studies over 21 days which reveal a bimodal delivery mechanism influenced by both GelMA degradation and electrical stimulation events. This data demonstrates an electroactive and cytocompatible material suitable for the delivery of protein payloads over 3 weeks. This material is well suited for use as a treatment delivery platform in tissue engineering applications where targeted and spatio-temporal controlled delivery of therapeutic proteins is required.

Statement of significance

Growth factor use in tissue engineering typically requires sustained and tunable delivery to generate optimal outcomes. While conducting polymer hydrogels (CPH) have been explored for the electrically responsive release of small bioactives, we report on a CPH capable of releasing a protein payload in response to electrical stimulus. The composite material combines the benefits of soft hydrogels acting as a drug reservoir and redox-active properties from the conducting polymer enabling electrical responsiveness. The CPH is able to sustain protein delivery over 3 weeks, with electrical stimulus used to modulate release. The described material is well suited as a treatment delivery platform to deliver large quantities of proteins in applications where spatio-temporal delivery patterns are paramount.

* Correspondence author.
E-mail address: d.svirskis@auckland.ac.nz (D. Svirskis).

https://doi.org/10.1016/j.actbio.2023.01.013
1742-7061/

Please cite this article as: E. Cheah, M. Bansal, L. Nguyen et al., Electrically responsive release of proteins from conducting polymer hydrogels, Acta Biomaterialia, https://doi.org/10.1016/j.actbio.2023.01.013

1. Introduction

The therapeutic peptide and protein class represents a significant market share in the current pharmaceutical sector and is amongst the fastest-growing categories of therapeutics. However, most protein-based therapeutics using direct delivery systems face major challenges. Therapeutic proteins have inherent *in vitro* and *in vivo* instability, illicit immunogenicity reactions and exhibit poor biodistribution to the diseased site, which all contribute to the high degrees of failure during the drug development cycle [1]. Despite this, since the 1980s, a total of 239 therapeutic proteins and peptides have been approved for clinical use by the United States Food and Drug Administration [2]. However, the vast majority of this progress has been made from the dominance of monoclonal antibody therapeutics, but not all protein drugs have seen success [3]. For example, recombinant growth factors (GF) therapeutics has experienced a drop off in interest in recent years, with no GF therapeutic products approved since 2014 [1]. GFs are soluble polypeptide molecules secreted by cells to regulate a multitude of cellular functions essential for healing. These signaling molecules are able to induce migration, proliferation, and differentiation post-injury, making them essential in directing regenerative pathways for many cell populations [4–6]. Therefore, GFs retain enormous potential in the field of tissue regeneration.

The limited success observed with GF mediated regeneration therapies is partly due to difficulties in achieving effective spatial and temporal presentation to cell surface receptors [7]. Most approved clinical GF releasing delivery systems use a form of a sustained release formulation in an effort to address this challenge. For example, the INFUSE^{TM} bone graft uses an absorbable collagen sponge to control the release of recombinant bone morphogenetic protein-2 (BMP-2). The sustained release of BMP-2 purportedly improves bone regeneration after injury [8]. However, this has not been without controversy, with conflicting studies about its effectiveness and concerningly, reports of complications and serious side effects [9]. In particular, patients treated with the INFUSE^{TM} bone graft was observed to have high rates of ectopic bone formation associated with leakage of BMP-2 outside the implant site with difficulties in identifying optimum dosages [10]. The story of the INFUSE^{TM} bone graft serves as a useful example to highlight the intricacy and complexity of utilizing GFs in regenerative medicine. There is a clear need for an approach with a highly targeted spatial and temporal delivery minimizing off-target exposure.

Electrically tunable delivery systems offer an interesting proposition to solve these challenges. A directly addressable release system using a safe electrical stimulus can facilitate the release of GF doses that can be spatiotemporally controlled to ensure the desired GF exposure to encourage tissue regeneration. To that end, a number of electrically responsive systems aimed at releasing growth factors have been studied over the last 2 decades, utilizing materials such as graphene oxide and conducting polymers (CP) [11,12].

One CP backbone of prominence is poly(3,4-ethylenedioxythiophene) (PEDOT), with wide applicability as a functional addition to existing bioelectronics in the form of electrode coatings [13]. PEDOT has drawn considerable attention in both academic and industrial applications due to its high conductivity and stability in ambient conditions [14]. PEDOT can be electrochemically synthesised on a conductive surface *in situ* from an aqueous monomer, 3,4-ethylenedioxythiophene (EDOT) and a supporting dopant. After electrodeposition of this electroactive polymer, electrical stimulation drives electrons into and out of the conjugated backbone, with mobile ions transported both within and exchanged with oppositely charged ions in the surrounding electrolyte to balance the net charge. This electrostatic property offers the possibility of on-demand dynamic release of a payload [15]. On-demand drug delivery using this property of PEDOT has been demonstrated for a variety of biologically relevant molecules, including dexamethasone, ciprofloxacin, nerve growth factor (NGF), and brain-derived neurotrophic factor (BDNF) [15–18]. Furthermore, the cytocompatibility and bio-stability of PEDOT has been well demonstrated in both *in vitro* and *in vivo* applications [19–22]. However, there are inherent limitations towards successful implementation of CPs. One main drawback of the CPs is the limited drug loading capacity. In a prior study of a polypyrrole CP, a maximum of 458.2 ng/cm^2 of nerve growth factor was reported to be loaded into the CP [23]. While an achievement, for longer term tissue engineering applications, larger amounts of GFs released over time is crucial to achieve tangible therapeutic effects [24]. The present study considers a modification of traditional CPs with the incorporation of a highly biocompatible hydrogel, forming a class known as conducting polymer hydrogels (CPH) [25,26]. CPHs have been explored for electrically controlled drug release applications, releasing small charged drug molecules such as dexamethasone [26,27]. The hydrogel component of the hybrid material provides a porous polymeric network which acts as a reservoir for drug release, increasing the total drug payload capacity. Furthermore, the added hydrogel component in some cases can provide increased biocompatibility, introduce biodegradability, and improve the biological interface of the CP [28]. Few studies have explored the release of proteins from a CPH. For example, Chikar et al. developed a PEDOT/alginate CPH loaded with BDNF as a cochlear electrode implant, however, the release mechanism of the BDNF was diffusion driven [18]. In another example, Cheong et al. developed a PEDOT/poly(vinyl alcohol) based conducting polymer hydrogel for the delivery of nerve growth factor [29]. Consequently, in this work, we aim to demonstrate a biocompatible electro-responsive CPH made by electropolymerizing PEDOT in a GelMA layer adhered to a conductive substrate, with the ability to dynamically control the release of proteins over weeks.

Gelatin-methacryloyl (GelMA) hydrogels comprise of functionalised gelatin, a relatively cheap and highly abundant protein derived from collagen. The gelatin is functionalised with methacrylic anhydride to impart the ability to crosslink in the presence of a photoinitator, allowing for tuneable physical properties and rapid gelation [30,31]. Furthermore, GelMA has been shown to support a wide range of cell types, presenting arginine-glycine-aspartic acid (RGD) motifs which promote cell attachment and spreading via integrin binding [32–34]. The ease of synthesis and versatility has made GelMA one of the most commonly used hydrogels for biomedical applications. Its biocompatible nature and high water swellability make it a good candidate to serve as an initial template for selective patterning and fabrication of the CPH.

In this study, the electrochemistry of the fabricated CPH is directly compared to plain PEDOT polymerised under the same conditions to understand how GelMA influences the hybrid material. Key parameters such as impedance, charge transfer properties and electroactive stability are assessed. We also confirm the cytocompatibility of the CPH with human cells. Finally, we demonstrate how electrical stimulation can modify the release of a model protein payload of bovine serum albumin (BSA) over 4 h, and then explore the release over an extended time frame of 3 weeks, demonstrating the ability of electrical stimulation to modulate release rates. BSA is a globular protein with an average molecular weight of 66.7 kDA, isoelectric point of ~4.5 and a hydrodynamic radius of 3.6 nm [35,36]. By way of example to enable comparison, a GF of interest for tissue regeneration applications is ciliary neurotrophic factor (CNTF) [37]. CNTF has a molecular weight of 23 kDA, an estimated isoelectric point of 6.35 and a calculated hydrodynamic radius of 2.47 nm [38,39]. While no model is perfect, BSA is a good candidate for proof-of-concept for the development of the drug delivery platform due to its similar physicochemical

properties compared to GFs, stability, low cost, and ease of quantification [23,40,41].

2. Methods and materials

2.1. Fabrication of gold substrates for material coatings

Gold substrates were patterned using conventional photolithography techniques from gold coated glass slides with a titanium adhesion layer (100 nm/ 40 nm) (Au/Ti) obtained commercially (Deposition Research Laboratories Incorporated, MO, USA). SU8 2005 (Microchem Corp., USA) was used to generate a 1 cm^2 square pattern with a thickness of 5 µm on the gold surface which acted as an overlying insulation layer and as a spacer for the GelMA hydrogel coatings [25]. These substrates were then used to evaluate the material and protein release performance. A custom substrate array with 4 independently addressable 0.5 cm^2 gold surfaces was further fabricated for Atomic Force Microscopy (AFM) characterizations and growth factor release experiments.

2.2. Cysteamine functionalization of gold surfaces to improve adherence

The method for the functionalization of the gold surface was adapted from He et al. [42]. Patterned gold surfaces were first cleaned and activated by oxygen plasma treatment, (45 W, 0.100 mBar, 2 min) (Harrick Plasma, NY, USA). These were then submerged into 1% (w/w) cysteamine in ethanolic solution and incubated at room temperature for 12 h under dark conditions. The substrates were then washed thrice with fresh ethanol solution to remove adsorbed cysteamine. The resulting cysteamine monolayer modified surfaces were then immersed into a 100 mM NaOH solution for 2 h to carry out a Michael-type reaction between the amino groups of cysteamine and the acrylate end groups of GelMA. Verification of this functionalization step has previously been reported by our group [25].

2.3. FITC-BSA conjugation and quantification for sustained release experiments

Bovine serum albumin (BSA) (pH Scientific, NZ) was labelled with fluorescein isothiocyanate (FITC) (Sigma Aldrich, Australia) in 0.1 M carbonate buffer (pH 9) at room temperature in the dark for 2 h with a 4:1 FITC to protein ratio. The Fluorescein isothiocyanate-Bovine Serum Albumin (FITC-BSA) solution was dialysed with a 14 kDa molecular weight cut-off cellulose membrane (Thermo Fisher, MA, US) against 0.01 M Phosphate Buffer Solution (PBS) (Sigma Aldrich, Australia), pH 7.4, at 37 °C for 24 h, then against deionized water for a further 2 h. The solution was then frozen at −20 °C overnight, and lyophilised. FITC-BSA was quantified by generating a calibration curve from 10 µg/ml to 15.625 ng/ml and measuring the fluorescence intensity of respective solutions using the Varioskan™ LUX Microplate Reader (ThermoScientific, USA) with an excitation wavelength of 490 nm and an emission wavelength of 525 nm.

2.4. GelMA hydrogel synthesis

The method to synthesize GelMA was adapted from Shirahama et al. [30]. Type A gelatin (6 g) (300 Bloom) (Sigma Aldrich, Australia) was dissolved in carbonate-bicarbonate buffer (60 ml, 0.1 M, pH 9). The gelatin solution was heated to 40 °C and 0.6 ml of methacrylic anhydride (Sigma Aldrich, Australia) was added dropwise to the gelatin solution over 10 min. The reaction was left to react at 40 °C for 3 h. The reaction was quenched by adjusting to pH 7 using 0.1 M HCl and was then centrifuged. The resulting supernatant was dialysed against deionized water at 37 °C for 7 days with daily water replenishing. Subsequently, the solution was frozen at −20 °C overnight and freeze dried (- 60 °C, 40 µBar). The resultant white foam was collected and stored at −20 °C until required for use.

A prepolymer solution (10 µl) consisting of 15% GelMA and 0.05% Igracure 2959 (98%) (Sigma Aldrich, Australia) was dispensed onto the cysteamine functionalised gold. A hydrophobic coverslip achieved by a coating of octadecyltrichlorosilane (>90%) (Sigma Aldrich, Australia) as previously described by Kirkpatrick et al. was used to flatten the hydrogel monomer droplet across the SU 8 patterned gold substrate [43]. The GelMA was then exposed to UV light (365 nm) for 2 min through a laser cut acrylic mask to allow for complete gelation of the hydrogel. To aid the lift-off of the coverslip the substrates were placed onto a heated 40 °C hot plate for 20 s, and then the coverslip was carefully lifted off the surface. The 5 µm SU 8 layer acted as a spacer, controlling the GelMA thickness to 5 µm. For protein release experiments, 1.2 mg/ml of FITC-BSA was added to the prepolymer solution prior to UV crosslinking.

2.5. Electrochemical deposition of PEDOT/pTS in CP and CPH samples

A three-electrode electrochemical cell was set up using either the hydrogel coated or plain gold as the working electrode, an aqueous Ag/AgCl reference electrode, and stainless-steel mesh as a counter electrode. Electrodeposition of PEDOT/*para*-Toluene Sulfonate (*p*TS) was accomplished by potentiostatic deposition from a 0.01 M EDOT (97%) (Sigma Aldrich, Australia) and 0.05 M Na *p*TS (95%, M_W = 194.19 mol/l) (Sigma Aldrich, Australia) aqueous solution using a potential of + 0.9 V. The total amount of charged passed was used to control and monitor the amount of PEDOT/*p*TS deposited within the CP and CPH samples. After each 100 mC of charge was deposited, polymerization was paused for 10 min to allow for diffusion of reactants into the hydrogel before restarting the electrodeposition. Each cycle was repeated 13 times to achieve a total charge density of 1300 mC/cm^2. To load the materials with protein, 1.2 mg/ml of FITC-BSA was added to the electropolymerization solution. During this step, the deposited PEDOT is in the oxidised and positive state, generating electrostatic attraction forces on the negatively charged FITC-BSA, leading to increased FITC-BSA loading within the polymer network. For plain PEDOT/*pTS* (in the absence of GelMA), to promote polymerization and adhesion it was necessary to electropolymerize 100 mC of non-protein loaded PEDOT/*p*TS first prior to a further 1200 mC of protein loaded PEDOT/*p*TS. Illustration of the CPH construction as shown in Fig. 1. All samples were washed thrice with Milli-Q water prior to any characterization or drug release experiments.

2.6. Investigating electrochemical characteristics of materials

All electrochemical characterizations were accomplished using a three-electrode electrochemical cell using the modified gold as a working electrode, an Ag/AgCl reference electrode, and a platinum mesh as a counter electrode. The electrolyte used was 0.01 M PBS solution. Cyclic voltammetry (CV) scans were conducted from +0.9 V to - 0.6 V at 100 mV/s. Afterwards, the cathodic charge storage capacity ($CSC_{cathodic}$) was calculated by determining the area of the CV curve during the cathodic sweep. Electrochemical impedance spectroscopy (EIS) was measured by applying a sinusoidal signal with 10 mV amplitude from a frequency range of 1 Hz to 10 kHz. Characterization of stability indicators were conducted over the span of the expected release profile of the drug delivery system. The CPH was submerged into a solution of 0.1 M PBS at 37 °C and 5% CO_2 over 21 days with solutions replaced daily. CV and EIS was measured on Day 0 and at Day 21. Additional stress

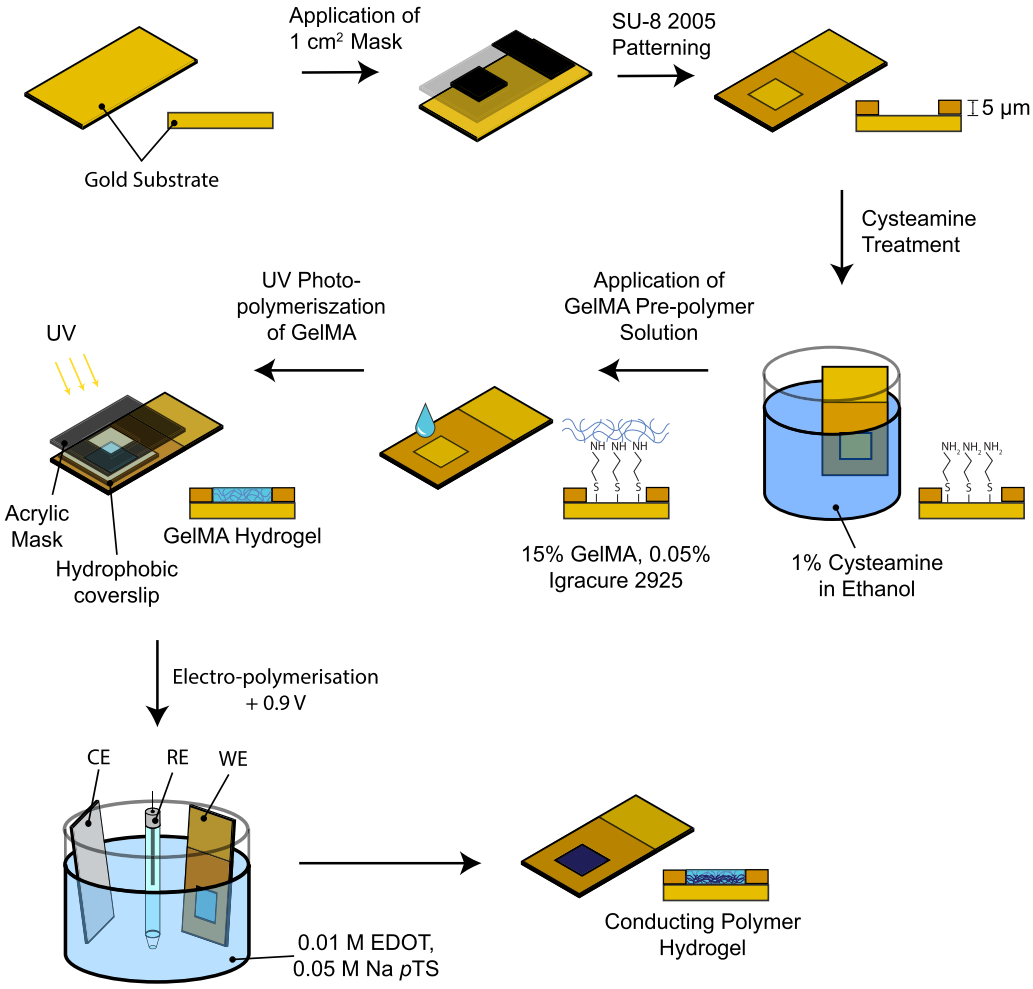

Fig. 1. Schematic representation of CPH coating construction. The gold substrate is first photolithographically patterned using SU-8 2005 to generate a 1 cm^2 area. The substrate is then functionalized with cysteamine. The GelMA pre-polymer solution is then dispensed onto the surface, flattened with a hydrophobic glass slide then exposed to UV crosslinking. A three-electrode setup with the counter electrode (CE) as a stainless-steel mesh, reference electrode (RE) as an aqueous Ag/AgCl reference electrode, and the working electrode (WE) as the gold substrate. Electropolymerization at +0.9 V in the electrodeposition solution is conducted electrochemically grow the PEDOT/pTS into the hydrogel to achieve the final CPH.

testing of CPH, PEDOT/*p*TS and GelMA was performed by subjecting the materials to continuous CV cycling between – 0.6 V and +0.9 V at a rate of 100 mV/s for 2000 cycles in 0.01 M PBS.

2.7. Examination of surface morphology and physical stability of CPH

Freshly prepared and incubated samples (0.01 M PBS at 37 °C for 7 and 21 days) of GelMA, CP and CPH were imaged using Scanning Electron Microscopy (SEM) to look at the surface morphology and cross-section. All samples were removed from the PBS, carefully blotted dry and dried overnight, then stored at – 20 °C prior to SEM analysis. For the cross-sectional analysis, the samples were fractured at room temperature, and the cross section imaged. The surface and cross-sectional samples were mounted and sputter coated with platinum (Polaron SC 7640 sputter coater). A Philips XL30 S field emission gun SEM was used to investigate the cross section with an accelerating voltage of 20 kV, spot magnification of 2.0, and magnifications from x 800 to x 35,000.

2.8. Probing CPH surface chemistry changes over time

FTIR was used to investigate the surface chemistry changes in the material over the timespan of protein release. FTIR spectra of the materials were obtained using Bruker Optics Tensor 37, Ettlingen, Germany in attenuated total reflectance (ATR) mode using a germanium ATR crystal. FTIR spectra were collected directly from the surface of the GelMA hydrogel, PEDOT/*p*TS, and CPH. Pristine, 7 day and 21 day samples were analysed for changes in surface chemistry over time. In order to obtain further spectra information on the CPH, shavings were collected by scraping the CPH from the gold surface and analysed. Prior to all analysis, the samples were placed into a vacuum oven at 40 °C for 30 min to remove water content. The spectra were obtained from a frequency range of 600 to 4000 cm^{-1} at a resolution of 4 cm^{-1} over 64 cumulative scans. Manual baseline correction and normalization to the largest peak were conducted for all spectra for analysis.

2.9. Examining the mechanical properties of CPH by atomic force microscopy

CPH and GelMA samples were incubated in 0.01 M PBS at 37 °C for 1, 7, and 21 days prior to mechanical analysis. AFM was performed using an MFP-3D Origin AFM (Asylum Research, Santa Barbara, USA) in a liquid environment at room temperature. Pre-calibrated borosilicate spheres (5 µm diameter) on silicon nitride cantilevers with spring constants ranging between 0.07 to 0.08 N/m were used for the force-indentation maps for day 1 and 21 CPH samples, and all GelMA samples. Force map sizes of a min-

imum of 10 × 10 indentation force curves were collected over a 400 μm^2 area using an indent velocity of 4 μm/s and a trigger point of 5 nN over a 2 μm force distance. For the 21-day CPH sample, a pre-calibrated triangle tip on a silicon nitride cantilever with spring constants ranging between 0.07 to 0.08 N/m were used. A force map size of 6 × 6 indentation force curves was collected over 400 μm^2 using an indent velocity of 1 μm/s and a trigger point of 200 nN over a 1.5 μm force distance. At least 4 force maps were obtained over each sample's area. Asylum Research software (Igor Pro, Wavemetrics) was used to apply fitting parameters with the Hertz model. A fit between 10 and 90% of the force applied were used to quantify the Young's modulus of the hydrogel and CPH samples from the force-indentation curves. The value of the Poisson's ratio for the gels were assumed to be 0.33 while for the Day 21 samples, a Poisson's ratio of 0.34 was used [44,45]. A histogram of the elastic modulus was generated for each force map and a Gaussian fit applied. Force curves within force maps displaying irregular shapes or values were excluded from the fit by applying mask that excluded the curves with a fit above or below a threshold value [46]. The data is presented as the mean value of the elastic modulus ± standard deviation as calculated by the Gaussian fit on the histogram of each force map.

2.10. Cytocompatibility assessment using neural precursor cells

Cytocompatibility of the CPH coating was assessed by exposing a 1 cm^2 CPH coated gold substrate to human induced neural precursor cells [47]. A modified 24 well culture lid with open slots was generated to vertically suspend the CPH coated gold slides into the 24 well cell culture plate containing human induced neural precursor cells. The CPH materials were generated as previously described, but with all starting materials sterilised through a 0.22 μm sterile filter. Furthermore, an additional sterility measure of a 2-hour soak in 70% ethanol was undertaken.

The cells were plated onto Geltrex-coated glass coverslips in a Nunc-treated 24-well plate for differentiation. At day 2 of differentiation, the cells were exposed to the CPH and cultured for a further 5 days. The cells grown without exposure to the CPH coatings acted as a control. Cell viability was then measured using a LIVE/DEAD© cell viability assay (Invitrogen, USA). Briefly, the cells were incubated in a solution of 2 μM calcein-AM and 4 μM ethidium homodimer (EthD-1) at room temperature for 40 min. Green fluorescent calcein AM indicates live cells and red fluorescent EthD-1 indicates dead cells. The labelled cells were then imaged using a Nikon TE2000E inverted fluorescent microscope and a 10X objective lens equipped with a GFP and Texas Red filter set. Seven images from different regions of each well were acquired across each of the three coverslips. Image analysis was performed using ImageJ to obtain the total number of live and dead cells [48]. The average percentage of cell viability was estimated as:

$$\frac{Number\ of\ Live\ Cells}{Total\ Number\ of\ Cells} * 100$$

2.11. Assessing electrical stimulus modulation of the FITC-BSA release

A pre-soak of 45 min was conducted for the removal of adsorbed protein from all samples. Electrical stimulated responsive release of FITC-BSA from the loaded hydrogel, PEDOT/*p*TS, and CPH was determined by releasing into an electrochemical cell filled with 2 ml of 0.01 M PBS (pH 7.4), where a trigger signal was applied for 4 h sampling every 15 min. To investigate the influence of constant potential on FITC-BSA release, samples were subjected to either a reducing −0.6 V, an oxidizing + 0.6 V, or biphasic pulses, determined against a Ag/AgCl reference electrode. Two different biphasic pulses were explored, both with an amplitude of ± 0.6 V, at a frequency of 0.1 Hz with a pulse width of 4 s, or a frequency of 0.01 Hz with a pulse width of 40 s. Passive release of FITC-BSA from the loaded hydrogels, PEDOT/*p*TS, and CPH was determined by immersion into 2 ml of 0.01 M PBS solution at room temperature for 4 h. For each sampling point, 300 μl of release media was removed and fluorescence measured against the FITC-BSA calibration curve. 300 μl of fresh PBS was added back to the release chamber as replacement.

2.12. Sustained stimulated release of FITC-BSA

Having determined effective electrical stimuli to modulate the release of FITC-BSA from the CPH materials, extended release was assessed by placing samples into 2 ml of 0.01 M PBS at 37 °C for 3 weeks. Samples of the media were taken every 24 h for the first 14 days. From days 15 to 21, the stimulated group was exposed to a potential controlled biphasic pulse with an amplitude of ± 0.6 V, pulse width of 4 s, at a frequency of 0.1 Hz for 1 h each day. These set of stimulation parameters were chosen due to being effective at inducing sufficient release, while being more conducive to cell survival due to the biphasic nature of the stimulation as opposed to a monophasic stimulation [49]. On the stimulatory days, samples of the release media were taken before and after each stimulation cycle. The maximum amount of protein that could be released from the CPH was determined by looking at the amount of protein released at day 21 from the stimulated CPH group. For comparison, FITC-BSA loaded GelMA was allowed to passively release into 2 ml of release media for 14 days, and the total released protein at this timepoint was determined as the maximum amount of protein releasable for GelMA hydrogels.

2.13. Statistics

Statistical significance of the $CSC_{cathodic}$, Young's modulus, cell viability assay and comparisons of FITC-BSA release was analysed using GraphPad Prism 8.2.1 software (GraphPad Software, USA). Statistical comparisons between different datasets were determined using an unpaired two-tailed *t*-test. Probabilities of $p \leq 0.05$ were determined as statistically significant.

3. Results and discussion

3.1. Preparation of CPH

In this study, a two-step fabrication process was used to prepare the conducting polymer hydrogel. The first step involves the adhesion and subsequent polymerization of the GelMA hydrogel via UV irradiation, and the second, an *in situ* electropolymerization of PEDOT/*p*TS through the initially formed hydrogel layer (Fig. 1). Through the use of lithographic techniques, the 5 μm thick Su-8 insulation layer doubles as a spacer to form the hydrogel. To maintain a smooth and uniform hydrogel, a hydrophobic glass slide was used to flatten and spread the hydrogel monomer solution across the gold. Covalent attachment of the GelMA hydrogel was achieved via cysteamine-gold anchoring. The verification of this process was previously demonstrated in our group [25]. The hydrogel matrix was soaked in an EDOT and *p*TS monomer solution, then PEDOT/*p*TS was electropolymerized from the conductive substrate into the hydrogel. While galvanostatic polymerization is usually preferred for PEDOT electropolymerization, it was found to be detrimental to the polymerization of PEDOT into the GelMA hydrogel, with delamination of the hydrogel common. Potentiostatic control resulted in more consistent and reliable polymerization of the PEDOT/pTS within the hydrogel. Electropolymerization of PEDOT/*p*TS (as determined by the rate of charge passed) was found to be significantly slower in the hydrogel compared to a plain gold

surface (total polymerization time of 8 h vs 2 h). This could be due to diffusion through the hydrogel layer being a limiting factor towards electropolymerization of the PEDOT/*p*TS.

3.2. Electrochemical performance of CPH

The electrochemical performance of the CPH compared to plain gold and PEDOT/*p*TS were evaluated using CV and EIS (Fig. 2). As expected, CVs of both the CP and CPH materials display an enlarged CV area compared to a plain gold surface (Fig. 2A). Consistent with previously reported results, the CV plot of the PEDOT/*p*TS displays a large rectangular CV curve with an almost featureless voltammetry plot with a small oxidation peak around – 0.05 V and a reduction peak at 0.65 V [21]. The increased CV area is indicative of high capacitive charge transfer property, corresponding to the increased electroconductive surface area as seen in SEM images, allowing for more charge transfer available for electrical stimulation [50]. The CV plot of the CPH coating closely mirrors the PEDOT/*p*TS plot, although with a moderate reduction in the geometric area in the CV. Two small oxidation peaks are observed in the CPH coatings at 0.1 and 0.2 V, alongside a two reduction peaks at 0.6 V and −0.15 V, indicative of faradaic process occurring. $CSC_{cathodic}$ values further illustrate the difference between the coatings, with the PEDOT/*p*TS and CPH displaying a 58.7 and 42.4-fold increase in the $CSC_{cathodic}$ compared to plain gold (Fig. 2B). This demonstrates that the CPH material has a higher charge transfer capacity compared to gold but not to the extent of the PEDOT/*p*TS material.

EIS measures are typically used for electrode characterization and as a parameter to monitor stability of electrode coatings [51]. The EIS data is in good agreement with the observations seen with the CV. The Bode plot (Fig. 2C) shows a decrease in |Z| magnitude impedance for both CPH and PEDOT/*p*TS compared to plain gold across the whole frequency range tested of 1 Hz to 10 kHz. However, the CPH coating displayed a slightly higher impedance than PEDOT/*p*TS but only within the low frequency ranges (10 Hz to 1 Hz). At these lower frequency ranges, the dominant charge transfer is of faradaic resistive quality, with surface reactions and other charge transfer mechanisms contributing to the impedance displayed [51].

The electrocharacterization results indicate the successful infiltration of PEDOT/*p*TS through the GelMA hydrogels generating a significant increase in charge transfer capacity as compared to a plain gold surface. However, it is noted that the addition of the GelMA hydrogel does slightly reduce the charge transfer capacity as compared to the unaltered CP. This is possibly due to the insulating nature of the GelMA hydrogel inhibiting a level of charge transfer.

Long term stability of the CPH material was assessed through incubation in 0.01 M PBS at 37 °C for a total of 21 days. Baseline and Day 21 electrochemical characterization measuring $CSC_{cathodic}$ and |Z| magnitude impedance at 1 kHz was undertaken to measure the potential loss of charge transfer capacity due to degradation over the expected time frame of drug delivery. $CSC_{cathodic}$ measures were taken to identify possible losses in charge transfer that occur over time, while |Z| magnitude impedance at 1 kHz is a regularly used measure of impedance characterization of neural electrodes [51]. In this particular application, the use of the |Z| magnitude impedance is used as a comparative performance measure highlighting a possible increase in resistances occurring at the 1 kHz frequency. As seen in Fig. 2D and E, no statistical difference was observed for any measure. Minor decreases in the $CSC_{cathodic}$ and |Z| impedance magnitude was observed. These results

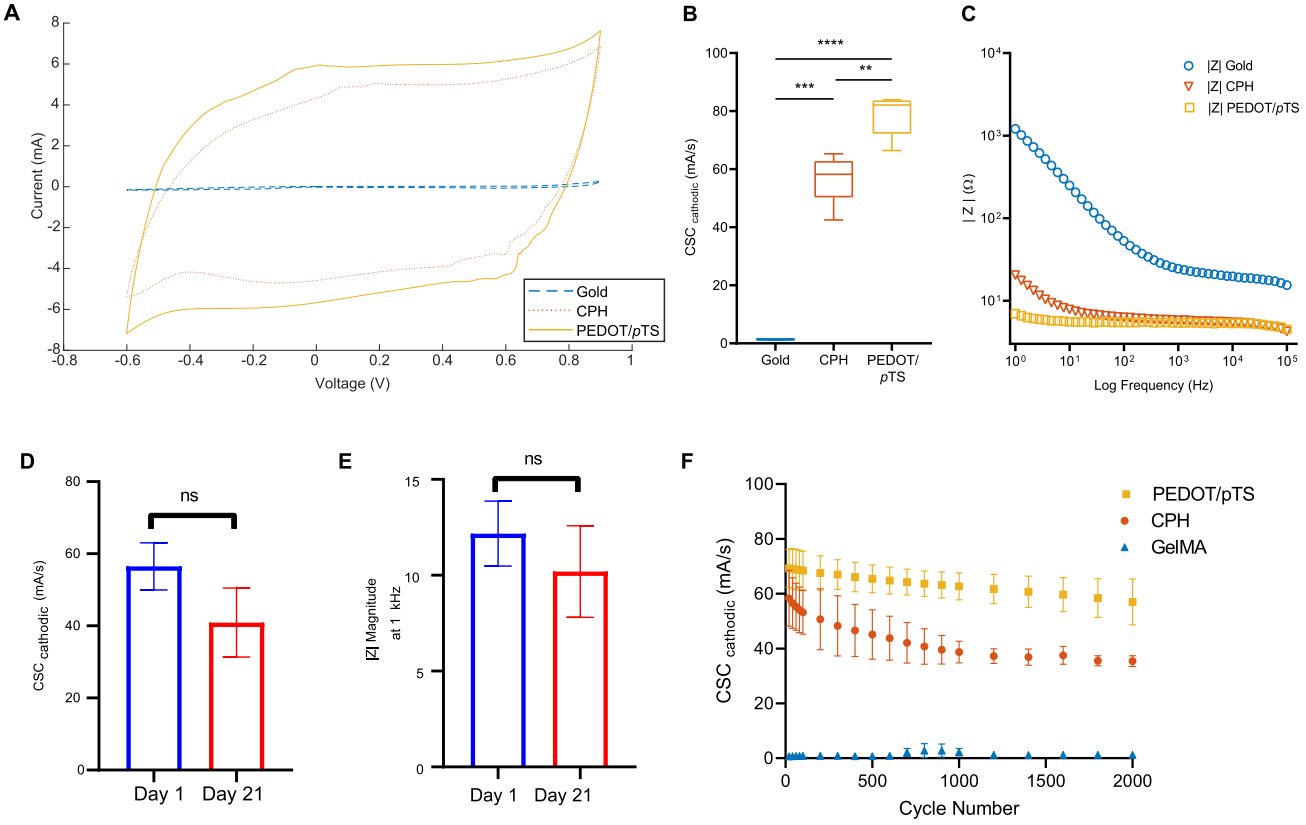

Fig. 2. Electrochemical characterization conducted of Gold, PEDOT/pTS, and CPH coatings, all measurements made against a Ag/AgI reference electrode. (A) Exemplary CV sweeps at cycle 10 for each material type. (B) Cathodic charge storage capacity of each material, as determined by CV sweeps ($n = 4$). Error bars denote standard deviation. (** $p < 0.01$, **** $p < 0.0001$). CPH performance over 21 days (D) CSCcathodic measured from cycle 7 of CV cycles across 21 days. (E) |Z| magnitude measure by EIS over 21 days. ($n = 3$) (F) Mean CSCcathodic of PEDOT/pTS, CPH, and GelMA over 2000 CV cycles in PBS. ($n = 3$).

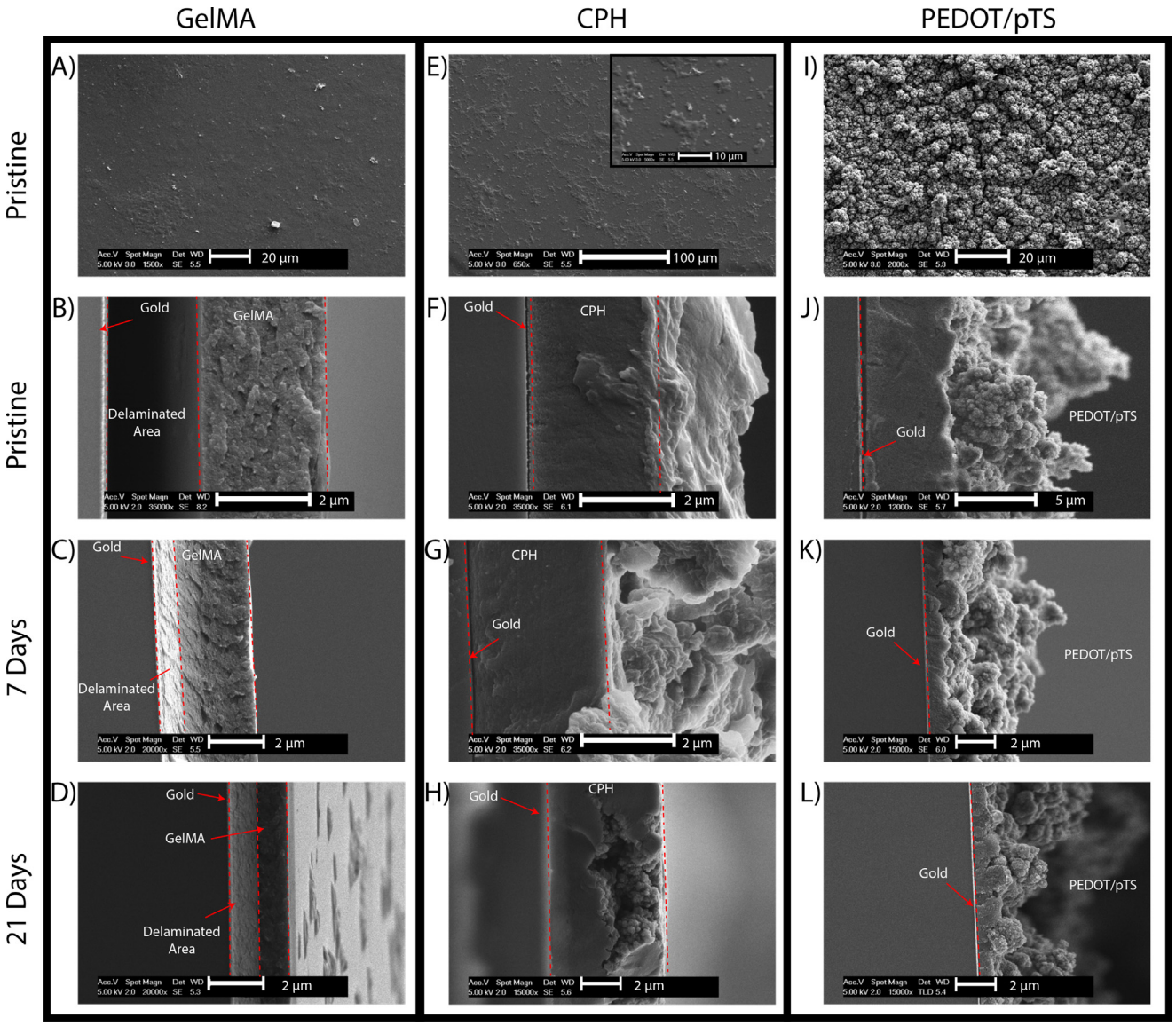

Fig. 3. SEM images obtained highlighting surface morphology and cross-sectional analysis of GelMA, CPH, and PEDOT/pTS. (A) Surface morphology of a pristine GelMA hydrogel showing a featureless gel layer. (B) Cross-section of a pristine hydrogel. (C) Cross-section of GelMA hydrogel incubated for 7 days. (D) Cross-section of GelMA hydrogel incubated for 21 days. (E) Surface morphology of a pristine CPH surface showing a smooth surface with granulations present, distinct from GelMA and PEDOT/pTS. (Inset depicts 5000 x magnification of surface). (F) Cross-section of pristine CPH showing the smooth undulating surface with a dense GelMA underlay at the gold surface. (G) Cross-section of CPH incubated for 7 days. (H) Cross-section of CPH incubated for 21 days, showing the interior granulated structure typical of PEDOT/pTS within the CPH. I) Surface morphology of pristine PEDOT/pTS showing typical granular, cauliflower-like morphology of PEDOT/pTS. (J) Cross-section of pristine PEDOT/pTS. (K) Cross-section of PEDOT/pTS incubated for 7 days. (L) Cross-section of PEDOT/pTS incubated for 21 days. (Scale bars as indicated in each micrograph.).

indicate the CPH is stable across a timeframe expected for drug delivery to occur, with no adverse effects to the charge transfer capacity. Additional electrochemical stability of the CPH material was evaluated by extensive CV cycling in PBS. During CV cycling, the materials experiences mechanical stress due to the repetitive expansion and contraction due to ionic changes caused by the oxidation and reduction of the material [52]. As seen in Fig. 2F, we observed a steady decrease in the $CSC_{cathodic}$ of PEDOT/*p*TS and the CPH with an increase in the number of CV cycles, eventually reaching a steady plateau after 1200 cycles. The decrease in $CSC_{cathodic}$ is associated with de-doping of the PEDOT with other anions in the PBS [25]. The reduction in $CSC_{cathodic}$ was more evident with the CPH material in comparison to the PEDOT/*p*TS, with a 36% decrease compared to a 26% decrease after 1200 cycles. This difference may be suggestive of changes associated with the degradation of some GelMA within the CPH. In contrast, no changes in the $CSC_{cathodic}$ were observed with the GelMA material. These results indicate that the CPH retains its electroactivity and is able to withstand electrochemical stresses expected during electrical stimulation.

3.3. Surface and cross-sectional morphology characteristics of CPH

Morphological characteristics of the GelMA hydrogel, PEDOT/*p*TS, and CPH coatings were examined by SEM. Fig. 3A highlights the surface morphology of the GelMA hydrogel displaying a near featureless smooth layer. The typical porous morphology of GelMA hydrogels was not seen during SEM analysis. One possible explanation of this is due to the hydrogel collapsing as the samples were not freeze dried prior to SEM (due to the risk of delamination from the gold substrate) [53]. Fig. 3B-D shows the cross-section of the dry GelMA hydrogel on Day 0, Day 7, and Day 21 of incubation at 37 °C. A rough estimation of the dried hy-

drogel thickness was obtained from the cross-sectional SEM images taken ($n = 1$). The dried hydrogel layer was observed to decrease in thickness over time with an estimated starting thickness of 2.8 µm reducing to 1.2 µm on Day 21 (Fig. 3B,D). Fig. 3I and J show the typical cauliflower-like rough granular morphology of the PEDOT/*p*TS coatings consistent with previously published literature [17]. No distinct morphology changes were noted for the PEDOT/*p*TS coatings after 21 days at 37 °C (Fig. 3J-L). The CPH coating shows a smooth surface with areas of apparent granulations distinct from both the smooth GelMA surface and rough granular PEDOT/*p*TS coatings (Fig. 3E). Cross-sectional images confirm this observation, with a dense underlay capped with a smooth undulating surface found on the CPH (Fig. 3F). The thickness of the dried CPH layer was observed to be approximately 2.6 µm. A reason for the unique surface feature observed on the CPH surface may be due to the electrodeposition of the PEDOT/*p*TS within the GelMA hydrogel. Electrochemical deposition of PEDOT generates the typical rough and bumpy morphology due to nucleation of transitioning EDOT monomers into oligomers at the electrode site [54]. These oligomers then coalesce and grow onto each other to form the solid PEDOT films. This discontinuous growth of PEDOT into the GelMA hydrogel may be the cause of the deformations noted on the surface. Degradation of the overlying layer of the CPH over 21 days at 37 °C revealed the previously dense underlay of the CPH contained rough cauliflower-like morphology typical of PEDOT/*p*TS (Fig. 3H). These observations support the idea of the successful formation of a semi-interpenetrating hybrid material coating, with the GelMA component partially degrading over 21 days. GelMA hydrogels have been reported previously to have very slow degradation rates in PBS solutions, requiring collagenase enzymes to induce biodegradation [34,55]. However, these studies on GelMA utilize bulk hydrogel formats, where small degradation effects would not be quantified accurately. In a thin film format, as shown by SEM, the degradation of the GelMA is apparent.

3.4. Spectral analysis of CPH

FTIR spectra analysis showed characteristic peaks within the GelMA hydrogel samples at 1640, 1530, 1450 and 1335 cm^{-1}, corresponding to amide I band, amide II band, C–H bending and O–H bending respectively (Fig. 4A). These peaks are also evident at the CPH surface. Within the PEDOT/*p*TS spectra, characteristic peaks are seen at 1510, 1306, 1184, 1083, 1049 and 674 cm^{-1} consistent with previous reports [56]. The bands at 1510 and 1306 cm^{-1} correspond to the asymmetric stretching mode of C=C and interring stretching of C–C. Bands at 1184, 1083 and 1049 cm^{-1} are attributed to the C–O-C bending vibrations within the ethylenedioxy group while bands at the 674 cm^{-1} region are characteristic of stretching vibrations of the C-S-C bond in the thiophene ring. No evidence of the PEDOT/*p*TS is initially seen when looking at the CPH surface, possibly as the ATR-FTIR penetration depth of a germanium crystal is limited to within 0.17 µm to 1.66 µm [57,58]. However, as the samples were stored over 21 days at 37 °C, peaks associated with PEDOT/*p*TS were observed, indicating some degradation of the GelMA component. Shavings of the CPH coating off the gold surface showed both characteristic peaks of the GelMA hydrogel and PEDOT/*p*TS. Slight peak shifts are noted, specifically, the movement of the PEDOT/*p*TS peaks of 1510 and 1306 cm^{-1}. This can be attributed to the close proximity of the GelMA peaks at 1530 and 1335 cm^{-1} respectively. In the spectra obtained of the 7 and 21 day incubated CPH coating, an almost identical spectrum to the CPH shavings was observed with characteristic peaks of both the GelMA hydrogel and the PEDOT/*p*TS present in these samples. The initial absence of PEDOT/*p*TS FTIR peaks on the surface of the day 1 CPH coating, and subsequent appearance after 7 days of incubation points to evidence of a semi-interpenetrating CPH, whereby the overlying GelMA component partially degrades over time, revealing the inner CPH comprising both PEDOT/*p*TS, and GelMA.

3.5. Mechanical properties of CPH determined by AFM

The mechanical properties of the CPH were explored using AFM force indentation. Force indentation maps of the CPH and the GelMA samples were performed on 1, 7, and 21 days of incubation in a solution of 0.01 M PBS at 37 °C. As seen in Fig. 4B, no significant differences were found between the GelMA and the CPH at Day 1, with an average Young's Modulus of 53.4 ± 17.6 kPA and 67.4 ± 29.8 kPA respectively. These results are in line with previously reported stiffness values of a 15% GelMA hydrogel found in the literature (~25 kPA to ~100 kPA) [59].

After 7 days of incubation however, we observed an increase of the Young's Modulus of the GelMA sample to 115.3 ± 36.7 kPA, while on day 21, the GelMA sample could not be accurately probed with the Young's Modulus being too high to probe with available cantilevers. The CPH also experienced an increase in stiffness after 7 days and 21 days, with an approximate 4-fold increase and a 9000-fold increase, respectively. These observations indicate the GelMA hydrogel has degraded in both the GelMA and CPH sam-

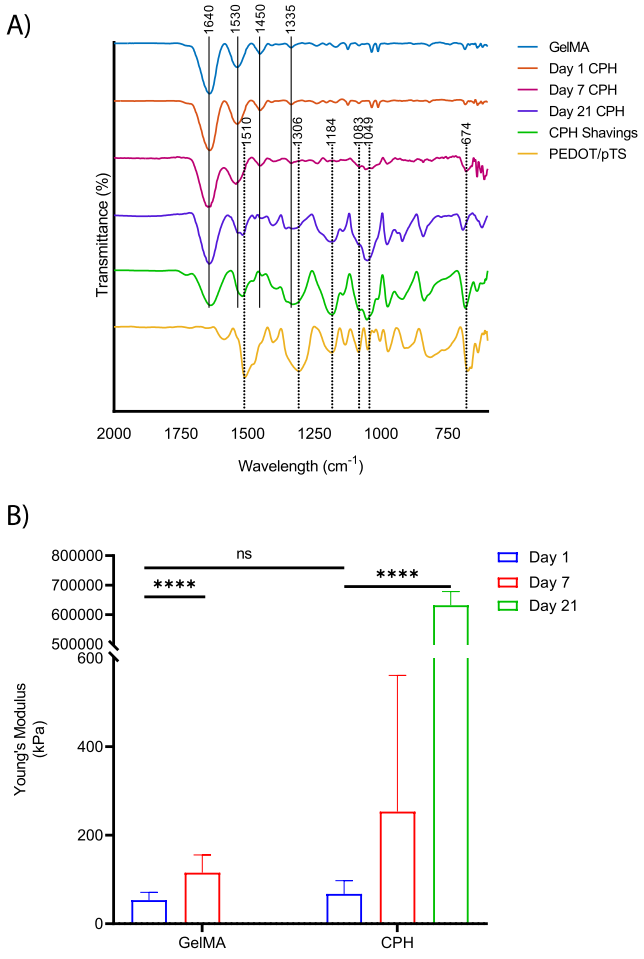

Fig. 4. (A) FTIR spectra of the GelMA hydrogel surface, CPH on Day 1, 7, and 21, CPH Shavings and PEDOT/pTS. Typical GelMA peaks denoted by thick dotted lines, and thin dotted lines correspond to PEDOT/pTS peaks. Spectra shown in the fingerprint frequency region of 2000 cm−1 to 600 cm−1. (B) Young's Modulus of GelMA hydrogel and CPH coatings at Day 1 and Day 7 and day 21 of incubation in 0.01 M PBS at 37 °C. Mean Young's Modulus obtained from Hertzian model fitted with a Gaussian distribution from 6 individual 8 × 8 force maps (Day 1 and 7 GelMA and CPH) and 4 individual 6 × 6 force maps (Day 21 CPH), (**** $p < 0.0001$).

ples by day 21. The increase in stiffness observed with the GelMA samples was likely influenced by the stiff underlying gold substrate with the 100 nm gold coated substrate having a reported Young's Modulus of approximately 56 GPa, leading to the difficulties encountered probing the samples [60]. Contrastingly, while the stiffness of the CPH coatings increased over this period of time, the Young's Modulus remained at ~630 MPa, an 88-fold decrease in the expected stiffness of the underlying substrate. Therefore, the stiffness values probed on day 21 of the CPH likely arose from the PEDOT/*p*TS component. Previously published results by Hassarati et al. on the stiffness for a hydrated PEDOT/*p*TS film suggests a stiffness in the range of ~ 150 MPa, with the discrepancy between the stiffness values obtained in this study due to differences in experimental set-up [61]. However, as force indentation only probes the surface of the material, and whilst we have observed the GelMA degrading from the surface of the CPH, there may still be GelMA left entrapped in the CP polymer network underneath, as reported with the SEM and FTIR analysis.

3.6. Cytocompatibility of CPH coatings

Cytocompatibility of the CPH coatings were verified by exposure of the CPH coatings to human induced neural precursor cells. These cells were chosen to assess compatibility of the CPH delivery system for the development of future neural regeneration therapies. The CPH coatings were incubated within the cell culture media for 5 days. Cell viability was determined after this point with a LIVE/DEAD© assay. Fig. 5A shows the representative fluorescence images of cells exposed to control or CPH material. Further image analysis (Fig. 5B) showed that after 7 days in culture, the control group had an average viability of 53± 4%, while the CPH exposed group had a viability of 64 ± 15%, displaying a non-significant difference between the control cells and treated cells. The level of cell viability observed in the control group is in good agreement with previous studies conducted with this cell type [62]. These results suggest that the CPH coatings exhibit no adverse effect towards cells and are consistent with previously published literature whereby the cytocompatibility of separate components (PEDOT/*p*TS and GelMA) are well established [26,34,63].

3.7. Electrical stimulation modulated release of FITC-BSA

In order to study the mechanisms driving electrically triggered release, the release of FITC-BSA from GelMA hydrogels, PEDOT/*p*TS, and CPH coatings were first studied over 4 h (240 min) with and without the influence of electrical triggers. GelMA hydrogels, PEDOT/*p*TS, and CPH coatings, all at 1 cm^2, loaded with FITC-BSA were immersed into PBS solutions for 240 min and the release of FITC-BSA was measured at different time points. The release samples were quantified by interpolating the fluorescence intensity with the generated calibration curve. The FITC-BSA calibration curve was found to be linear between 10 µg/ml and 15.625 ng/ml (R^2=0.995). FITC-BSA loading into the GelMA hydrogel was achieved by direct mixing and incorporation into the GelMA prepolymer solution, entrapping the proteins directly within the polymeric network. BSA has an isoelectric point of around 4.5, making it slightly negatively charged in the electropolymerization solution of EDOT and *p*TS (pH 6.5). During the electropolymerization of PEDOT/*p*TS at a constant oxidizing potential of + 0.9 V, electrostatic interactions would attract the FITC-BSA to the forming PEDOT which is in an oxidised state with a net positive charge. The CPH coating utilizes both aforementioned loading steps to incorporate the FITC-BSA within the GelMA/PEDOT/*p*TS network, resulting in a 3-fold increase in the maximum amount releasable compared to the GelMA hydrogel (34 ± 10 µg vs 11 ± 2 µg) (Fig. S1).

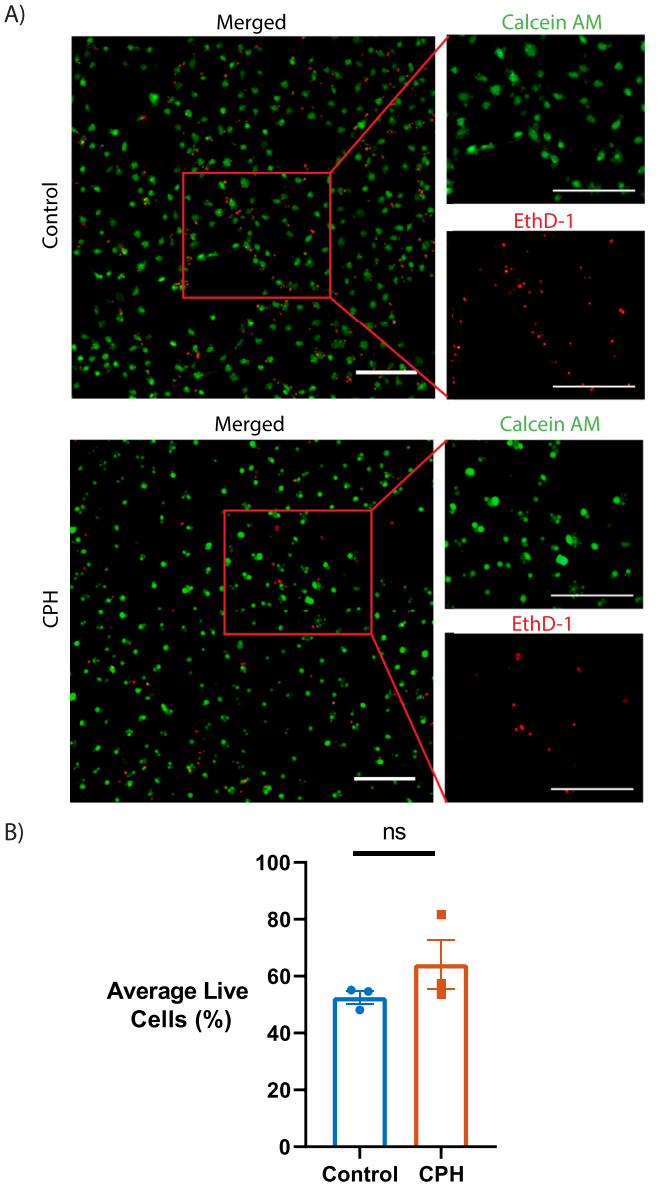

Fig. 5. Cytocompatibility of the CPH coatings evaluated using a LIVE/DEAD© cell viability assay on human induced neural precursor cells after 7 days in culture. (A) Representative fluorescence images taken using a 10X objective lens. (Scale bar 200 µm) (B) Bar graph showing the average percentage of live cells from three coverslips with seven images obtained from each coverslip. Each data point depicts the average percentage of live cells in each coverslip. Data represents as mean ± SEM.

Assessment of *in vitro* passive release (Fig. 6A) suggests steady release from all three materials over 240 min. The GelMA and CPH samples tended towards a higher initial burst of release, perhaps due to the highly hydrated nature of the materials facilitating diffusion. No statistical difference in the levels of raw protein release were observed for GelMA and CPH after the 240 min (6 ± 1 µg and 6 ± 1 µg), (representing 57% and 18% of the total amount of protein available for release). This indicates the initial release kinetics of the CPH is likely influenced by the overlying GelMA layer. The total FITC-BSA released from these two coatings were roughly 30% more than the PEDOT/*p*TS coatings (4.3 ± 0.3 µg) ($p < 0.05$) (Fig. 6E).

In order to investigate the ability for electrical stimulation to modulate release, comparisons of FITC-BSA release from the CPH material subjected to either a constant reduction potential of -0.6 V or a constant oxidation potential of + 0.6 V over 240 min

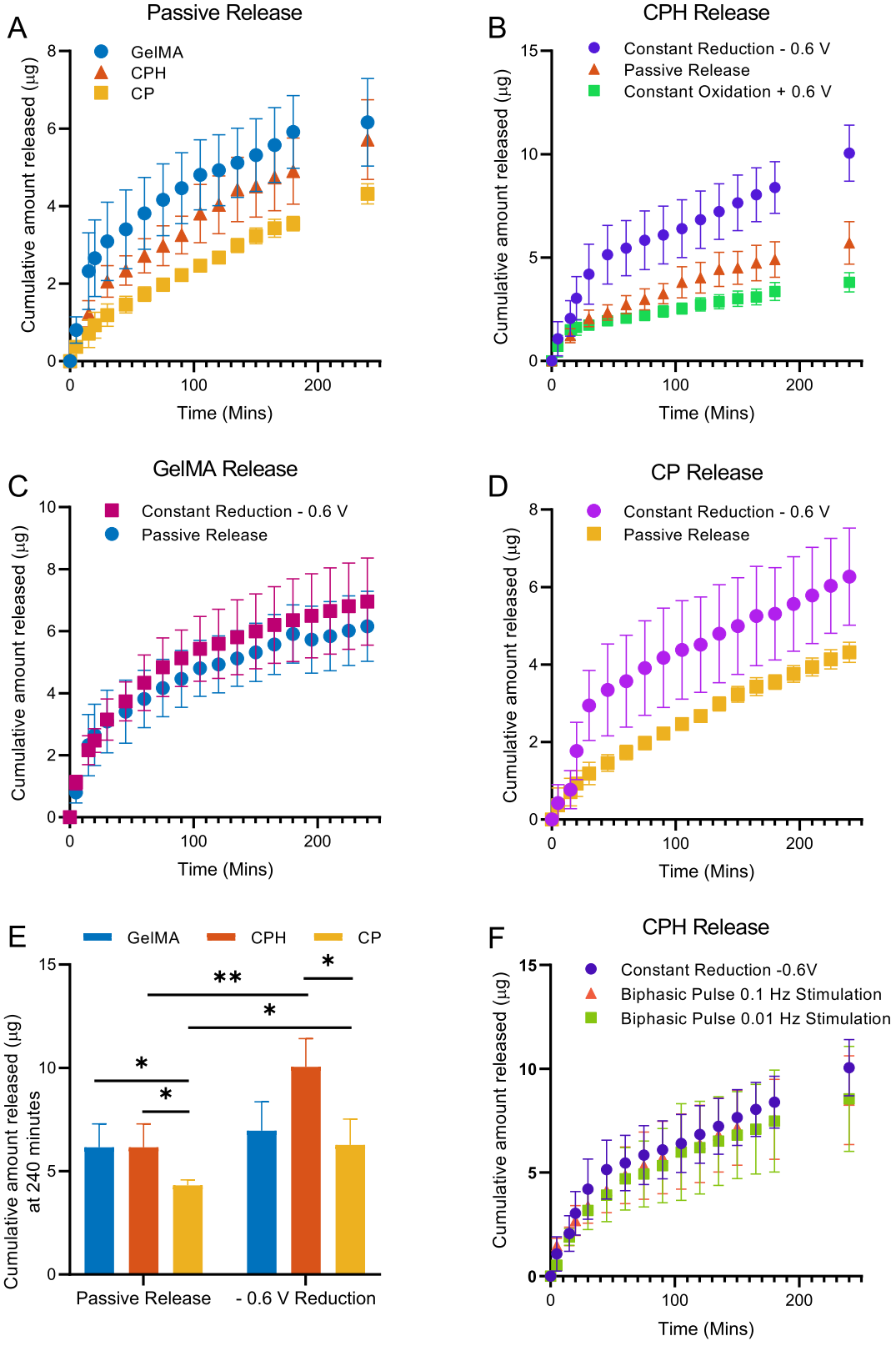

Fig. 6. Release kinetics of FITC-BSA over 240 mins from GelMA, CPH, and CP. Passive diffusion from GelMA, CPH and CP (A). A comparison of a constant potential of + 0.6 V or −0.6 V with passive diffusion from FITC-BSA loaded CPH (B) and for GelMA hydrogel (C) and CP (D). Total cumulative release at 240 min for each material (E). Effects of potential controlled biphasic pulses at 0.1 and 0.01 Hz against a constant potential of 0.6 V release from CPH (F). ($n = 4$) (* $P < 0.05$, ** $p < 0.01$).

were conducted (Fig. 6B). These potentials were chosen as the stimulation parameters to modulate the release of FITC-BSA from the CPH due to prior published literature exhibiting good control over the release of a small negatively charged glutamate from the CPH [25]. As seen in the CVs obtained in Fig. 2A this value is well under the observed reduction peaks that occur with these materials and ensures the material is in the reduced state. More extreme potentials beyond −0.6 V and + 0.6 V versus Ag/AgCl may cause unwanted electrochemical reactions such as water electrolysis that generate damage to the tissue and the CPH coatings [64,65]. Conversely, potentials closer to 0 V may (or may not) be efficient at generating the necessary stimulation required to trigger the release of the payload. As seen in Fig. 6B, a constant potential of - 0.6 V led to a 63% increase in the total amount released compared to passive diffusion (10.1 ± 1.4 µg vs 6.2 ± 1.1 µg) ($p < 0.05$). Applying a constant oxidation potential on the other hand, led to a 38% decrease in the total amount released (3.8 ± 0.6 µg vs 6.2 ± 1.1 µg) ($p < 0.05$). The negative potential applied electrochemically reduces the PEDOT, shifting the polymer backbone to a neutral state, and the *p*TS anions in the material would lead to an overall negative charge, resulting in the repulsion of the similarly charged FITC-BSA from the polymeric network. Applying a positive or oxidative potential reverses this mechanism, generating electrostatic attraction forces between the positively charged

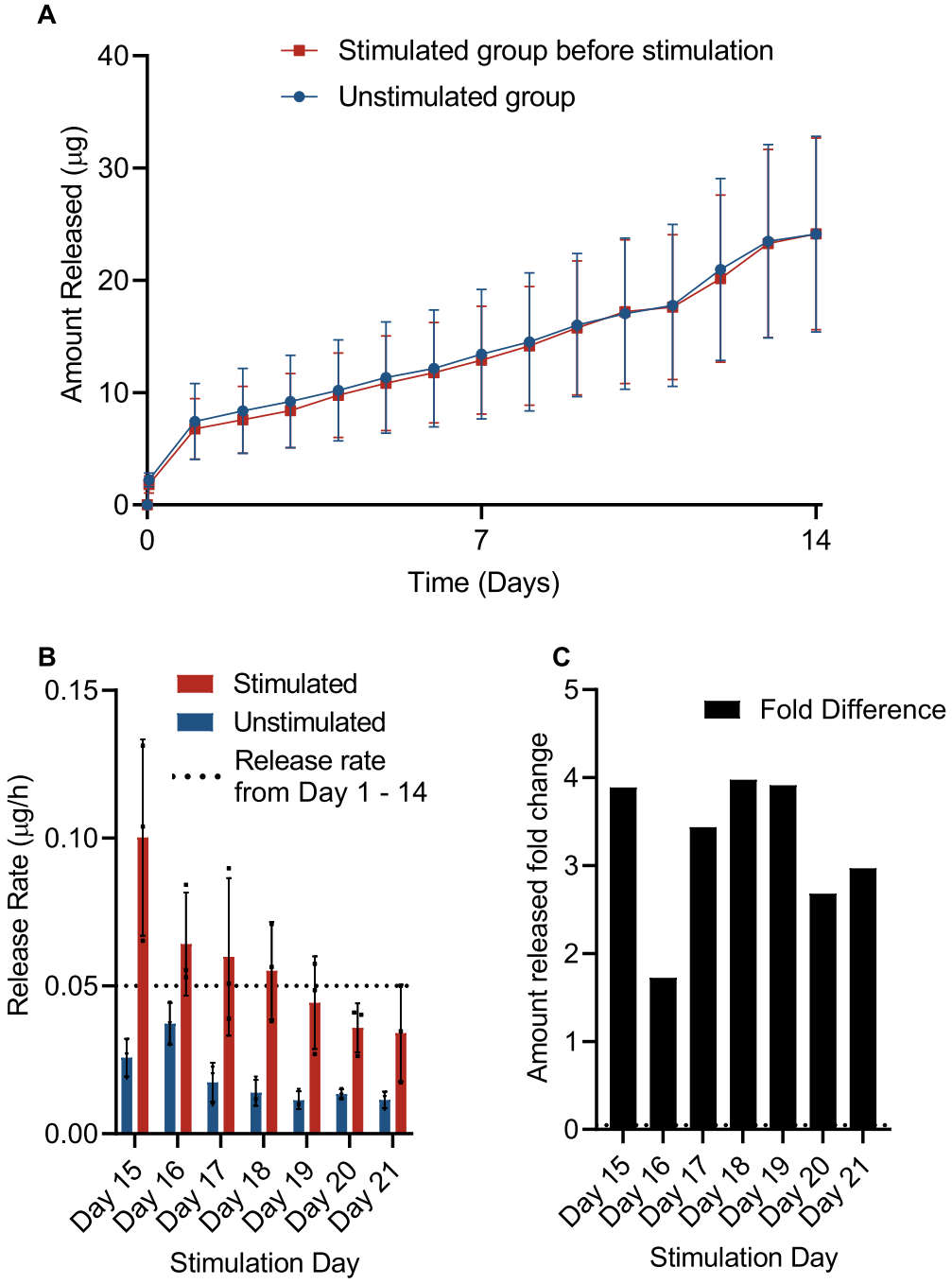

Fig. 7. (A) Cumulative release of FITC-BSA from the CPH coating over 14 days, sampled every 24 h, showing the passive release profile. (B) Difference in release rate between stimulated and unstimulated group on days 15 to 21. Active stimulation was conducted using a biphasic 0.6 V pulse at 0.1 Hz for 1 h once a day. Release rate from day 1 to 14 indicated by dotted line. Data points indicate individual release rates. (C) Fold change in the amount released between stimulated and unstimulated groups for each stimulation event on days 15 to 21. ($n = 3$) (Error Bars represent standard deviation).

PEDOT backbone and the negatively charged FITC-BSA resulting in slower release of the protein. This electrostatic control is not absolute, with diffusion driving forces still present within the system, leading to a baseline amount of FITC-BSA being released.

To isolate and confirm the electro-responsive characteristics of the individual components a constant - 0.6 V stimulation was applied independently to the GelMA hydrogel and PEDOT/*p*TS (Fig. 6C, D). GelMA is a hydrophilic polymer network that is not electroactive, and as expected, no significant differences in FITC-BSA release were observed between electrical stimulation and passive release of the GelMA samples. In comparison, stimulating the conductive PEDOT/*p*TS films displayed a 45% increase in the total amount released (6.3 ± 1.3 µg vs 4.3 ± 0.3 µg), however, the total amount released by the stimulation remained lower than the amount released with the CPH. This observation may be explained as the PEDOT/*p*TS polymeric network is not as water swellable compared to the GelMA and CPH, and may have been loaded with lower amounts of the water soluble FITC-BSA. These results confirm the electro-responsive characteristics displayed from the CPH arise from the incorporation of the PEDOT/*p*TS component.

Next, we explored the application of biphasic voltage-controlled pulses as a stimulatory driver for the release of FITC-BSA. The samples were either exposed to a 0.6 V biphasic stimulation at 0.1 Hz or 0.01 Hz for 240 min. As seen in Fig. 6E, no significant difference in the amount released were noted between the frequencies of the biphasic stimulation, or between the biphasic pulses and the constant −0.6 V stimulation.

Translation of uni-polar electrical fields *in vivo* settings for tissue stimulation purposes has been shown to be generally unsafe [66–68]. Application of prolonged monophasic stimulation may cause detrimental effects by generating irreversible faradaic reactions which in turn can (1) have destructive effects on the material itself and to the surrounding tissue by creating substantial pH changes through water electrolysis, and (2) generate possible side reactions leading to leeching of toxic metals into the body [51,67]. Furthermore, extended overstimulation of excitable tissue may induce cell death through the depletion of oxygen or glucose and changes in intracellular and extracellular ionic concentrations. *In vivo* applications of stimulating electrodes typically use and favor a biphasic charge-balanced signal for the aforementioned reasons, where the charge injected at the first phase is compensated for in the secondary phase, creating a net zero charge transfer [69,70]. The use of potentiostatic control as the trigger for protein release may decrease the risk of tissue damage through the regulation of the potential at the electrode surface, whilst being effective at triggering drug release. The use of biphasic potential controlled pulses reduces these risks further, providing an avenue for charge balancing to occur. For these reasons, the 0.1 Hz biphasic stimulation was chosen for further experiments.

3.8. Long term tunable release of FITC-BSA

In order to explore a sustained release model with a delayed stimulation onset, two groups of (stimulated, unstimulated) FITC-BSA loaded CPH samples were immersed into a 0.01 M PBS solution at 37 °C for a total of 21 days. Neither group received any stimulation over the first 14 days with the release profiles shown in Fig. 7A. In the first 24 h, an initial burst release was observed, which then lead into a zero-order kinetic release from day 1 to day 14, with a release rate of 0.05 µg/h ($r^2 = 0.9748$) (signified by the dotted line in Fig. 7B). No significant differences between the two groups were seen in the total amount of FITC-BSA released before stimulation was applied on day 15, 24.6 ± 8.8 µg vs 25.1 ± 8.8 µg ($p < 0.05$). From day 15 onwards the stimulated group was exposed to a biphasic ± 0.6 V amplitude at a frequency of 0.1 Hz, for 1 hour once a day, for a total of 7 stimulation events. The release rate in Fig. 7B was calculated from the difference in amount released between daily timepoints divided by the time elapsed from days 15 to 21 for each sample. Electrical stimulation was found to increase the average release rate after each stimulation event by approximately 3-fold compared to the unstimulated group (Fig. 7B). A gradual decrease in the release rate over this time was observed, possibly due to the depletion of the protein in the polymer matrix. However, the rate at day 21 remained high, 0.01 µg/h (Unstimulated) vs 0.03 µg/h (Stimulated). The differences in the release rate modulated by the electrical stimulus translates to a 3-fold increase in total amount released across the seven days (9.4 ± 1.2 µg vs 3.1 ± 0.6 µg) ($p < 0.05$) (Fig. 7C). These experiments exemplify the long-term utility of controlling the delivery of a protein over 21 days. Through the application of an electrical stimulus, the release rate can be modulated.

4. Conclusion

In this study, we report on the fabrication and characterization of a semi-interpenetrating CPH material coating comprising of a GelMA hydrogel and a PEDOT conducting polymer for the electrical stimulated release of a protein. Mechanical, chemical and SEM analysis revealed a semi-penetrating CPH network with an overlying layer of GelMA hydrogel that partially degrades over 21 days to reveal a fully interpenetrating network of GelMA and PEDOT/*p*TS. The cytocompatible material coating demonstrated a high degree of charge transfer capacity, whilst retaining the desirable mechanical and chemical characteristics of GelMA hydrogels. Electrically tunable control over the release rate of a model protein, FITC-BSA was established over 4 h and 21 days. The present study focusses on the characterization of the CPH material while demonstrating the utility as a platform to deliver protein, with release rates modifiable through electrical stimulation. While the described CPH material has the potential to deliver a range of proteins, further optimization is expected to tailor the material interactions with the specific protein based on a range of properties, including payload size and charge. Nonetheless, the protein delivery system described provides a promising material for the spatial and temporal targeted delivery of therapeutic proteins.

Ethics and integrity statement

Data will be made available on reasonable request. The authors declare no conflicts of interests to disclosed.

Declaration of Competing Interest

The authors declare that they have no known competing financial interests or personal relationships that could have appeared to influence the work reported in this paper.

Acknowledgments

EC acknowledges a supporting scholarship from the Vernon Tews Educational Trust. This work was supported by the HRC / CatWalk Trust Research Partnership (19/895), and DS acknowledges a Sir Charles Hercus Health Research Fellowship (19/007), both from the Health Research Council, New Zealand.

Supplementary materials

Supplementary material associated with this article can be found, in the online version, at doi:10.1016/j.actbio.2023.01.013.

References

[1] G. Walsh, Biopharmaceutical benchmarks 2018, Nat. Biotechnol. 36 (2018) 1136–1145, doi:10.1038/nbt.4305.
[2] S.S. Usmani, G. Bedi, J.S. Samuel, S. Singh, S. Kalra, P. Kumar, A.A. Ahuja, M. Sharma, A. Gautam, G.P.S. Raghava, THPdb: database of FDA-approved peptide and protein therapeutics, PLoS One 12 (2017), doi:10.1371/journal.pone.0181748.
[3] J.R. Kintzing, M.V. Filsinger Interrante, J.R. Cochran, Emerging strategies for developing next-generation protein therapeutics for cancer treatment, Trends Pharmacol. Sci. 37 (2016) 993–1008, doi:10.1016/j.tips.2016.10.005.
[4] V.S. Boyce, L.M. Mendell, Neurotrophins and spinal circuit function, Front. Neural Circuits. 8 (2014), doi:10.3389/fncir.2014.00059.
[5] A. Shpichka, D. Butnaru, E.A. Bezrukov, R.B. Sukhanov, A. Atala, V. Burdukovskii, Y. Zhang, P. Timashev, Skin tissue regeneration for burn injury, Stem Cell Res. Ther. 10 (2019) 1–16, doi:10.1186/s13287-019-1203-3.
[6] C. Blanpain, E. Fuchs, Plasticity of epithelial stem cells in tissue regeneration, Science 344 (2014) (80–.)1242281–1242281, doi:10.1126/science.1242281.
[7] A.C. Mitchell, P.S. Briquez, J.A. Hubbell, J.R. Cochran, Engineering growth factors for regenerative medicine applications, Acta Biomater. 30 (2016) 1–12, doi:10.1016/j.actbio.2015.11.007.
[8] Bone Grafting - OMF - Infuse Bone Graft | Medtronic, (n.d.). https://www.medtronic.com/us-en/healthcare-professionals/products/oral-maxillofacial-dental/bone-grafting/infuse-bone-graft.html (accessed June 7, 2022).
[9] J.W. Hustedt, D.J. Blizzard, The controversy surrounding bone morphogenetic proteins in the spine: a review of current research, Get. Good Res. Integr. Biomed. Sci. 87 (2018) 9–22.
[10] A.W. James, G. LaChaud, J. Shen, G. Asatrian, V. Nguyen, X. Zhang, K. Ting, C. Soo, A review of the clinical side effects of bone morphogenetic protein-2, Tissue Eng. - Part B Rev. 22 (2016) 284–297, doi:10.1089/ten.teb.2015.0357.
[11] D. Svirskis, J. Travas-Sejdic, A. Rodgers, S. Garg, Electrochemically controlled drug delivery based on intrinsically conducting polymers, J. Control. Release. 146 (2010) 6–15, doi:10.1016/j.jconrel.2010.03.023.
[12] A. Magaz, M.D. Ashton, R.M. Hathout, X. Li, J.G. Hardy, J.J. Blaker, Electroresponsive silk-based biohybrid composites for electrochemically controlled growth factor delivery, Pharmaceutics 12 (2020) 1–12, doi:10.3390/pharmaceutics12080742.
[13] C. Boehler, Z. Aqrawe, M. Asplund, Applications of PEDOT in bioelectronic medicine, Bioelectron. Med. 2 (2019) 89–99, doi:10.2217/bem-2019-0014.
[14] M.N. Gueye, A. Carella, J. Faure-Vincent, R. Demadrille, J.P. Simonato, Progress in understanding structure and transport properties of PEDOT-based materials: a critical review, Prog. Mater. Sci. 108 (2020) 100616, doi:10.1016/j.pmatsci.2019.100616.
[15] C. Boehler, F. Oberueber, M. Asplund, Tuning drug delivery from conducting polymer films for accurately controlled release of charged molecules, J. Control. Release. 304 (2019) 173–180, doi:10.1016/j.jconrel.2019.05.017.
[16] D. Esrafilzadeh, J.M. Razal, S.E. Moulton, E.M. Stewart, G.G. Wallace, Multifunctional conducting fibres with electrically controlled release of ciprofloxacin, J. Control. Release. 169 (2013) 313–320, doi:10.1016/j.jconrel.2013.01.022.
[17] R.A. Green, N.H. Lovell, L.A. Poole-Warren, Impact of co-incorporating laminin peptide dopants and neurotrophic growth factors on conducting polymer properties, Acta Biomater. 6 (2010) 63–71, doi:10.1016/j.actbio.2009.06.030.
[18] J.A. Chikar, J.L. Hendricks, S.M. Richardson-Burns, Y. Raphael, B.E. Pfingst, D.C. Martin, The use of a dual PEDOT and RGD-functionalized alginate hydrogel coating to provide sustained drug delivery and improved cochlear implant function, Biomaterials 33 (2012) 1982–1990, doi:10.1016/j.biomaterials.2011.11.052.
[19] M. Asplund, E. Thaning, J. Lundberg, A.C. Sandberg-Nordqvist, B. Kostyszyn, O. Inganäs, H. Von Holst, Toxicity evaluation of PEDOT/biomolecular composites intended for neural communication electrodes, Biomed. Mater. 4 (2009) 045009, doi:10.1088/1748-6041/4/4/045009.
[20] Z. Aqrawe, B. Wright, N. Patel, Y. Vyas, J. Malmstrom, J.M. Montgomery, D. Williams, J. Travas-Sejdic, D. Svirskis, The influence of macropores on PEDOT/PSS microelectrode coatings for neuronal recording and stimulation, Sens. Actuators B Chem. 281 (2019) 549–560, doi:10.1016/j.snb.2018.10.099.
[21] A.R. Harris, S.J. Morgan, J. Chen, R.M.I. Kapsa, G.G. Wallace, A.G. Paolini, Conducting polymer coated neural recording electrodes, J. Neural Eng. 10 (2013) 016004, doi:10.1088/1741-2560/10/1/016004.
[22] K. Krukiewicz, A. Kowalik, D. Czerwinska-Glowka, M.J.P. Biggs, Electrodeposited poly(3,4-ethylenedioxypyrrole) films as neural interfaces: cytocompatibility and electrochemical studies, Electrochim. Acta. 302 (2019) 21–30, doi:10.1016/j.electacta.2019.02.023.
[23] J. Jin, Z. Huang, G. Yin, A. Yang, S. Tang, Fabrication of polypyrrole/proteins composite film and their electro-controlled release for axons outgrowth, Electrochim. Acta 185 (2015) 172–177, doi:10.1016/j.electacta.2015.10.123.
[24] K. Lee, E.A. Silva, D.J. Mooney, Growth factor delivery-based tissue engineering: general approaches and a review of recent developments, J. R. Soc. Interface 8 (2011) 153–170, doi:10.1098/rsif.2010.0223.
[25] M. Bansal, B. Raos, Z. Aqrawe, Z. Wu, D. Svirskis, An interpenetrating and patternable conducting polymer hydrogel for electrically stimulated release of glutamate, Acta Biomater. (2021), doi:10.1016/j.actbio.2021.10.010.
[26] M. Bansal, A. Dravid, Z. Aqrawe, J. Montgomery, Z. Wu, D. Svirskis, Conducting polymer hydrogels for electrically responsive drug delivery, J. Control. Release. 328 (2020) 192–209, doi:10.1016/j.jconrel.2020.08.051.
[27] M. Nourbakhsh, P. Zarrintaj, S.H. Jafari, S.M. Hosseini, S. Aliakbari, H.G. Pourbadie, N. Naderi, M.I. Zibaii, S.S. Gholizadeh, J.D. Ramsey, S. Thomas, M. Farokhi, M.R. Saeb, Fabricating an electroactive injectable hydrogel based on pluronic-chitosan/aniline-pentamer containing angiogenic factor for functional repair of the hippocampus ischemia rat model, Mater. Sci. Eng. C 117 (2020) 111328, doi:10.1016/J.MSEC.2020.111328.
[28] B. Weng, J. Diao, Q. Xu, Y. Liu, C. Li, A. Ding, J. Chen, Bio-interface of conducting polymer-based materials for neuroregeneration, Adv. Mater. Interfaces 2 (2015) 1500059, doi:10.1002/admi.201500059.
[29] G.L. Mario Cheong, K.S. Lim, A. Jakubowicz, P.J. Martens, L.A. Poole-Warren, R.A. Green, Conductive hydrogels with tailored bioactivity for implantable electrode coatings, Acta Biomater. 10 (2014) 1216–1226, doi:10.1016/j.actbio.2013.12.032.
[30] H. Shirahama, B.H. Lee, L.P. Tan, N.J. Cho, Precise tuning of facile one-pot gelatin methacryloyl (GelMA) synthesis, Sci. Rep. 6 (2016) 1–11, doi:10.1038/srep31036.
[31] A.R. Spencer, A. Primbetova, A.N. Koppes, R.A. Koppes, H. Fenniri, N. Annabi, Electroconductive gelatin methacryloyl-PEDOT:PSS composite hydrogels: design, synthesis, and properties, ACS Biomater. Sci. Eng. 4 (2018) 1558–1567, doi:10.1021/acsbiomaterials.8b00135.
[32] S.S. Suri, F. Rakotondradany, A.J. Myles, H. Fenniri, B. Singh, The role of RGD-tagged helical rosette nanotubes in the induction of inflammation and apoptosis in human lung adenocarcinoma cells through the P38 MAPK pathway, Biomaterials 30 (2009) 3084–3090, doi:10.1016/j.biomaterials.2009.02.014.
[33] L. Zhang, F. Rakotondradany, A.J. Myles, H. Fenniri, T.J. Webster, Arginine-glycine-aspartic acid modified rosette nanotube-hydrogel composites for bone tissue engineering, Biomaterials 30 (2009) 1309–1320, doi:10.1016/j.biomaterials.2008.11.020.
[34] K. Yue, G. Trujillo-de Santiago, M.M. Alvarez, A. Tamayol, N. Annabi, A. Khademhosseini, Synthesis, properties, and biomedical applications of gelatin methacryloyl (GelMA) hydrogels, Biomaterials 73 (2015) 254–271, doi:10.1016/j.biomaterials.2015.08.045.
[35] K.A. Majorek, P.J. Porebski, A. Dayal, M.D. Zimmerman, K. Jablonska, A.J. Stewart, M. Chruszcz, W. Minor, Structural and immunologic characterization of bovine, horse, and rabbit serum albumins, Mol. Immunol. 52 (2012) 174–182, doi:10.1016/j.molimm.2012.05.011.
[36] H.P. Erickson, Size and shape of protein molecules at the nanometer level determined by sedimentation, gel filtration, and electron microscopy, Biol. Proced. Online 11 (2009) 32–51, doi:10.1007/s12575-009-9008-x.
[37] H. Shen, Z.L. Shen, P.H. Zhang, N.L. Chen, Y.C. Wang, Z.F. Zhang, Y.Q. Jin, Ciliary neurotrophic factor-coated polylactic-polyglycolic acid chitosan nerve conduit promotes peripheral nerve regeneration in canine tibial nerve defect repair, J. Biomed. Mater. Res. Part B Appl. Biomater. 95 (2010) 161–170, doi:10.1002/jbm.b.31696.
[38] C. Escartin, P. Hantraye, N. Déglon, Transplants of CNTF-producing cells for the treatment of Huntington's disease, Cell. Transplant. (2007) 385–398, doi:10.1016/B978-012369415-7/50023-5.
[39] CNTF (human), (n.d.). https://www.phosphosite.org/proteinAction?id=3509093&showAllSites&true (accessed July 12, 2022).
[40] J. Panyam, M.M. Dali, S.K. Sahoo, W. Ma, S.S. Chakravarthi, G.L. Amidon, R.J. Levy, V. Labhasetwar, Polymer degradation and *in vitro* release of a model protein from poly(D,L-lactide-co-glycolide) nano- and microparticles, J. Control. Release. 92 (2003) 173–187, doi:10.1016/S0168-3659(03)00328-6.
[41] S. Murdan, Electro-responsive drug delivery from hydrogels, J. Control. Release. 92 (2003) 1–17, doi:10.1016/S0168-3659(03)00303-1.
[42] L. He, D. Lin, Y. Wang, Y. Xiao, J. Che, Electroactive SWNT/PEGDA hybrid hydrogel coating for bio-electrode interface, Colloids Surf. B Biointerfaces 87 (2011) 273–279, doi:10.1016/j.colsurfb.2011.05.028.
[43] R. Kirkpatrick, C.L. Muhlstein, Performance and durability of octadecyltrichlorosilane coated borosilicate glass, J. Non. Cryst. Solids 353 (2007) 2624–2637, doi:10.1016/j.jnoncrysol.2007.05.013.
[44] G.N. Greaves, A.L. Greer, R.S. Lakes, T. Rouxel, Poisson's ratio and modern materials, Nat. Mater. 10 (2011) 823–837, doi:10.1038/nmat3134.
[45] U. Lang, N. Naujoks, J. Dual, Mechanical characterization of PEDOT:PSS thin films, Synth. Met. 159 (2009) 473–479, doi:10.1016/j.synthmet.2008.11.005.
[46] A.E. Chalard, A.W. Dixon, A.J. Taberner, J. Malmström, Visible-light stiffness patterning of GelMA hydrogels towards *in vitro* scar tissue models, Front. Cell Dev. Biol. 0 (2022) 1422, doi:10.3389/FCELL.2022.946754.
[47] B. Connor, E. Firmin, A. McCaughey-Chapman, R. Monk, K. Lee, S. Liot, J. Geiger, C. Rudolph, K. Jones, Conversion of adult human fibroblasts into neural precursor cells using chemically modified mRNA, Heliyon 4 (2018) e00918, doi:10.1016/j.heliyon.2018.e00918.
[48] C.A. Schneider, W.S. Rasband, K.W. Eliceiri, NIH Image to ImageJ: 25 years of image analysis, Nat. Methods 9 (2012) 671–675, doi:10.1038/nmeth.2089.
[49] D.R. Merrill, M. Bikson, J.G.R. Jefferys, Electrical stimulation of excitable tissue: design of efficacious and safe protocols, J. Neurosci. Methods 141 (2005) 171–198, doi:10.1016/j.jneumeth.2004.10.020.
[50] S.J. Wilks, S.M. Richardson-Burns, J.L. Hendricks, D.C. Martin, K.J. Otto, Poly(3,4-ethylenedioxythiophene) as a micro-neural interface material for electrostimulation, Front. Neuroeng. 2 (7) (2009), doi:10.3389/neuro.16.007.2009.
[51] C. Boehler, S. Carli, L. Fadiga, T. Stieglitz, M. Asplund, Tutorial: guidelines for standardized performance tests for electrodes intended for neural interfaces and bioelectronics, Nat. Protoc. 15 (2020) 3557–3578, doi:10.1038/s41596-020-0389-2.

[52] C. Boehler, F. Oberueber, S. Schlabach, T. Stieglitz, M. Asplund, Long-term stable adhesion for conducting polymers in biomedical applications: Irox and nanostructured platinum solve the chronic challenge, ACS Appl. Mater. Interfaces 9 (2017) 189–197, doi:10.1021/acsami.6b13468.
[53] H.I. Muri, L. Hoang, D.R. Hjelme, Mapping nanoparticles in hydrogels: a comparison of preparation methods for electron microscopy, Appl. Sci. 8 (2018) 2446, doi:10.3390/app8122446.
[54] V. Subramanian, D.C. Martin, Direct observation of liquid-to-solid phase transformations during the electrochemical deposition of poly(3,4-ethylenedioxythiophene) (PEDOT) by liquid-phase transmission electron microscopy (LPTEM), Macromolecules 54 (2021) 6956–6967, doi:10.1021/acs.macromol.1c00404.
[55] M. Rizwan, G.S.L. Peh, H.P. Ang, N.C. Lwin, K. Adnan, J.S. Mehta, W.S. Tan, E.K.F. Yim, Sequentially-crosslinked bioactive hydrogels as nano-patterned substrates with customizable stiffness and degradation for corneal tissue engineering applications, Biomaterials 120 (2017) 139–154, doi:10.1016/j.biomaterials.2016.12.026.
[56] Q. Zhao, R. Jamal, L. Zhang, M. Wang, T. Abdiryim, The structure and properties of PEDOT synthesized by template-free solution method, Nanoscale Res. Lett. 9 (2014) 1–9, doi:10.1186/1556-276X-9-557.
[57] S.G. Kazarian, K.L.A. Chan, ATR-FTIR spectroscopic imaging: recent advances and applications to biological systems, Analyst 138 (2013) 1940–1951, doi:10.1039/c3an36865c.
[58] R. Minnes, M. Nissinmann, Y. Maizels, G. Gerlitz, A. Katzir, Y. Raichlin, Using attenuated total reflection-fourier transform infra-red (ATR-FTIR) spectroscopy to distinguish between melanoma cells with a different metastatic potential, Sci. Rep. 7 (2017) 1–7, doi:10.1038/s41598-017-04678-6.
[59] A.K. Miri, H.G. Hosseinabadi, B. Cecen, S. Hassan, Y.S. Zhang, Permeability mapping of gelatin methacryloyl hydrogels, Acta Biomater 77 (2018) 38–47, doi:10.1016/j.actbio.2018.07.006.
[60] C. Birleanu, M. Pustan, V. Merie, R. Müller, R. Voicu, A. Baracu, S. Craciun, Temperature effect on the mechanical properties of gold nano films with different thickness, IOP Conf. Ser. Mater. Sci. Eng. 147 (2016) 012021, doi:10.1088/1757-899X/147/1/012021.
[61] R.T. Hassarati, J.A. Goding, S. Baek, A.J. Patton, L.A. Poole-Warren, R.A. Green, Stiffness quantification of conductive polymers for bioelectrodes, J. Polym. Sci. Part B Polym. Phys. 52 (2014) 666–675, doi:10.1002/polb.23465.
[62] L. Nguyen, Optimising the Use of GelMA Hydrogel to Enhance the Survival and Differentiation of Human Induced Lateral Ganglionic Eminence Precursor Cells, The University of Auckland, 2021 Embargoed.
[63] S. Baek, R.A. Green, L.A. Poole-Warren, Effects of dopants on the biomechanical properties of conducting polymer films on platinum electrodes, J. Biomed. Mater. Res. - Part A. 102 (2014) 2743–2754, doi:10.1002/jbm.a.34945.
[64] S.F. Cogan, Neural stimulation and recording electrodes, Annu. Rev. Biomed. Eng. 10 (2008) 275–309, doi:10.1146/annurev.bioeng.10.061807.160518.
[65] S.F. Cogan, K.A. Ludwig, C.G. Welle, P. Takmakov, Tissue damage thresholds during therapeutic electrical stimulation, J. Neural Eng. 13 (2016) 021001, doi:10.1088/1741-2560/13/2/021001.
[66] R. Vatsyayan, D. Cleary, J.R. Martin, E. Halgren, S.A. Dayeh, Electrochemical safety limits for clinical stimulation investigated using depth and strip electrodes in the pig brain, J. Neural Eng. 18 (2021), doi:10.1088/1741-2552/ac038b.
[67] S.B. Brummer, J. McHardy, M.J. Turner, Electrical stimulation with pt electrodes: trace analysis for dissolved platinum and other dissolved electrochemical products, Brain. Behav. Evol. 14 (1977) 10–22, doi:10.1159/000124611.
[68] W.M. Grill, J.T. Mortimer, Stimulus waveforms for selective neural stimulation, IEEE Eng. Med. Biol. Mag. 14 (1995) 375–385, doi:10.1109/51.395310.
[69] S. De Jesus, M.S. Okun, K.D. Foote, D. Martinez-Ramirez, J.A. Roper, C.J. Hass, L. Shahgholi, U. Akbar, A. Wagle Shukla, R.S. Raike, L. Almeida, Square biphasic pulse deep brain stimulation for Parkinson's Disease: the BiP-PD study, Front. Hum. Neurosci. 13 (2019) 368, doi:10.3389/fnhum.2019.00368.
[70] J.K. Krauss, N. Lipsman, T. Aziz, A. Boutet, P. Brown, J.W. Chang, B. Davidson, W.M. Grill, M.I. Hariz, A. Horn, M. Schulder, A. Mammis, P.A. Tass, J. Volkmann, A.M. Lozano, Technology of deep brain stimulation: current status and future directions, Nat. Rev. Neurol. 17 (2021) 75–87, doi:10.1038/s41582-020-00426-z.